DOI: 10.13009/EUCASS2017-144

A model for solid propellant burning fluctuations using mesoscale simulations

Stany GALLIER, Mathieu PLAUD***
Airbus Safran Launchers, 91710 Vert-le-petit, France
**stany.gallier@airbussafran-launchers.com*
***mathieu.plaud@airbusafran-launchers.com*

Abstract

The combustion of composite solid propellants shows velocity fluctuations which are expected to have marked effects on turbulence or aeroacoustic instabilities. In this work, we propose a specific propellant boundary condition that models such fluctuations using a spectral synthetic turbulence approach. In order to feed this model with reliable input data, we consider mesoscale direct simulations of propellant combustion. This new propellant boundary condition is implemented in a CFD flow solver and applied to a real lab-scale motor. Simulations show that burning fluctuations can trigger aeroacoustic instabilities, in better agreement with experiments.

1. Introduction

Numerical simulations are now widely used in the community of solid propulsion [1-4]. In such simulations, the solid propellant combustion is always somewhat idealized inasmuch as it is generally modeled as a prescribed mass rate which is constant in time and space. In reality, composite propellants are heterogeneous at microscale and their combustion gives rise to local fluctuations of gas velocity and temperature that are space- and time-correlated. Such local small-scale fluctuations are referred to as “combustion noise” in the rest of the paper. Note that although self-explanatory, this latter term is misleading in the sense that it is not related to acoustics. It will be however retained in this work for convenience.

The objective of this work is to account for this combustion noise in order to increase the relevance and reliability of simulations of solid motors. Taking into account some fluctuations at the propellant boundary conditions is expected to improve our modeling and understanding of turbulence or flow instabilities. Turbulence in injection-driven flows - like a solid motor - is not completely understood so far and shows complex features due to the massive blowing from propellant combustion [5-7]. Numerical simulations suggest that fluctuations at propellant surface (basically, injected turbulence) have a strong impact on the unsteady flow in a motor [8]. The growing interest of Large Eddy Simulation (LES) also requires the most energetic scales to be explicitly described, especially in the vicinity of the propellant surface.

In this work however, we will focus on a common flow instability in rockets referred to as parietal vortex shedding (PVS) and study how it can be triggered by combustion noise. Parietal vortex shedding is a powerful source of instability in rockets motors and it involves large coherent vortical structures convected by the mean flow [4,9,10]. It is an intrinsic injection-driven flow instability characterized by a finite number of discrete modes. The modes are temporally damped and spatially amplified in the axial direction. The fact that modes are damped in time suggests that a continuous perturbation is needed for this instability to develop. Such perturbations inherently exist in real motors but this is not likely to be the case in simulations because of ideal assumptions (spatially constant mass flow, perfectly smooth geometries, etc.). It is therefore common in simulations to add artificial unphysical perturbations (like some non-injecting cells on the propellant boundary condition) in order to trigger PVS. We believe that accounting for a more realistic boundary condition describing the propellant could help trigger PVS and compare more favorably to experiments without the need of computational artifacts.

This study proposes a model for propellant combustion noise. In Section 2, we describe such a model which we choose to be a spectral synthetic turbulence approach. This model requires some space and time characteristics of unsteady velocity which are inherently linked to propellant combustion. Therefore, in Section 3, we present some mesoscopic direct simulations of propellant combustion in order to evaluate such input data. The resulting model is implemented in a CFD solver as a specific boundary condition and we eventually present, in Section 4, some

DOI: 10.13009/EUCASS2017-144

applications to a subscale motor. Note that this study complements a related work [11] but models, propellants and applications are much different here. In particular, the present work focuses on how a PVS can be triggered by propellant fluctuations.

This work was carried out in the frame of a research project dedicated to thrust oscillations in solid rocket motors in collaboration with the French Space Agency CNES.

2. Combustion noise model

Because composite propellants are heterogeneous, their combustion displays some space and time-correlated fluctuations at the burning surface. Those fluctuations are primarily imposed by the largest burning particles (usually, Ammonium Perchlorate (AP)) that are typically O(100 µm). Flame stand-off distances are usually small, typically hundreds of µm. Therefore, length scales involved in propellant combustion are smaller than a typical grid spacing used in simulations of actual motors. This means that for motor simulations, propellant combustion is a surface process that cannot be explicitly described by usual grids. Beyond the propellant flame, chemical reactions are terminated and the flow can be described by the usual non-reactive Navier-Stokes equations. As a consequence, a fluctuation model based on synthetic turbulence is expected to be relevant. The idea of synthetic turbulence is central in aerodynamics – especially for LES or DNS – in which turbulence scales must be resolved. There is a large amount of work regarding reliable boundary conditions for turbulence and we will here rely on a spectral synthetic turbulence model developed by Davidson [12] as described in the following section.

2.1 Synthetic turbulence model

Following Davidson et al. [12,13], the velocity fluctuation **u**' is decomposed into a sum of *N* random Fourier modes in physical space as

$$\mathbf{u}'(\mathbf{r}) = 2\sum_{n=1}^{N} \hat{u}^n \cos(\boldsymbol{\kappa}^n.\mathbf{r} + \psi^n).\boldsymbol{\sigma}^n \qquad \textbf{(1)}$$

where $\hat{u}^n, \psi^n$ and $\boldsymbol{\sigma}^n$ are respectively the amplitude, phase and direction of Fourier mode *n* and **r** is the position vector in space. For each mode *n*, the unit wave vector $\boldsymbol{\kappa}^n$ is chosen randomly on the unit sphere (see [12,13] for more details). For an incompressible flow – which is the case in motor chambers where Mach number is typically 10^{-2} – we have $\nabla.\mathbf{u} = 0$. When applied to Eq.(1), we can show that $\boldsymbol{\kappa} . \boldsymbol{\sigma} = 0$, i.e. wave vector and velocity are orthogonal, from which we can deduce $\boldsymbol{\sigma}^n$ once $\boldsymbol{\kappa}^n$ is chosen. The phase ψ^n is taken as a random number uniformly on the range $[0, 2\pi]$. The amplitude of each mode $\hat{u}^n$ is taken from a classical equilibrium turbulence spectrum. A modified von Karman spectrum is considered [12,13] as

$$E(\kappa) = c_E \frac{u_{rms}^2}{\kappa_e} \frac{(\kappa/\kappa_e)^4}{\left[1+(\kappa/\kappa_e)^2\right]^{17/6}} e^{\left[-2(\kappa/\kappa_\eta)^2\right]} \qquad \textbf{(2)}$$

with c_E=1,45 and κ_η is the wave number of the Kolmogorov scale. The wave number κ_e corresponds to the most energetic scales, having length scale Λ_e.

The velocity fluctuations given by Eq. (1) can be computed at any position **r** but have zero time correlation so far. In order to introduce some time correlation, Davidson [12] introduced an asymmetric time filter by computing velocity at iteration *m* by

$$\tilde{\mathbf{u}}'^{m}(\mathbf{r}) = \alpha\, \tilde{\mathbf{u}}'^{m-1}(\mathbf{r}) + \beta\, \mathbf{u}'(\mathbf{r}) \qquad \textbf{(3)}$$

where **u'**(**r**) is the random velocity obtained from the above procedure Eq.(1). This fluctuation $\tilde{\mathbf{u}}'^{m}$ now contains some time correlation and is the quantity used in the combustion noise model. Coefficient α is taken to $\alpha=\exp(-\Delta t/\Lambda_t)$ where Λ_t is an integral time scale that must be prescribed and Δt is the simulation time step. Ensuring variance conservation ($\langle\tilde{u}'^2\rangle = \langle u'^2\rangle$) imposes $\beta = (1-\alpha^2)^{0.5}$.

2.2 Numerical Implementation

We here sum up the procedure, which basically consists of the following steps:

1. Specify wave number range

DOI: 10.13009/EUCASS2017-144

A wave number range [κ_1 ; κ_2] must be first selected. A usual choice in turbulence is $\kappa_1=\kappa_e/2$ and $\kappa_2=\kappa_\eta$. An integral length scale Λ_e is more intuitive to prescribe and the relation $\kappa_e=9/55\pi\, c_E\, /\Lambda_e$ can be further used for a turbulence in equilibrium.

2. Discretize wave numbers

The interval [κ_1 ; κ_2] is discretized into N modes of equal size $\Delta\kappa=(\kappa_2-\kappa_1)/N$. Our tests show that N=300 is generally enough.

3. Unit vectors

For each mode $n \in [1 ; N]$, random unit vectors $\boldsymbol{\kappa}^n$ and $\boldsymbol{\sigma}^n$ as well as phase ψ^n are randomly chosen.

4. Velocity amplitude

For a given spectrum $E(\kappa)$ (Eq. 2), the velocity amplitude for each mode can be computed using $\hat{u}^n = [\, E(\kappa).\Delta\kappa\,]^{1/2}$.

5. Velocity fluctuations

Fluctuations $\mathbf{u'}(\mathbf{r})$ are computed from Eq. (1) at any position $\mathbf{r}$.

6. Time correlation

Actual velocity fluctuation $\tilde{\mathbf{u}}'^{m}(\mathbf{r})$ at iteration m is computed from Eq. (3), for any position $\mathbf{r}$, knowing its value at the previous iteration $\tilde{\mathbf{u}}'^{m-1}(\mathbf{r})$.

7. Superposition to mean flow

Velocity $\tilde{\mathbf{u}}'^{m}(\mathbf{r})$ has zero space and time average and is added to the mean prescribed velocity $\bar{\mathbf{u}}(\mathbf{r})$ to get the "noisy" velocity $\mathbf{u}^m(\mathbf{r})= \bar{\mathbf{u}}(\mathbf{r}) + \tilde{\mathbf{u}}'^{m}(\mathbf{r})$.

All this procedure is implemented as a new boundary condition in our in-house flow solver CPS [1,14]. The obtained "noisy" velocity is directly imposed in each cell adjacent to the propellant boundary and at each iteration. This modified boundary condition is implemented in 2D/3D and is fully parallelized. We have also implemented a noise on the temperature although it will not be addressed in the frame of this paper.

The forthcoming mesoscale simulations, confirmed by simulations from Massa et al. [11] as well, show that during propellant combustion, velocity fluctuations are mostly normal to the surface and tangential fluctuations are much smaller (typically 5-10 times smaller). Therefore, the fluctuation procedure will only be applied to that velocity component normal to the surface.

2.3 Input data and examples

The above model requires to specify three important input data regarding velocity fluctuations, namely :

- Integral time scale Λ_t (in Eq. 3)
- Integral length scale Λ_e (in Eq. 2)
- Fluctuation amplitude u_{rms} (in Eq.2)

Unfortunately, such data cannot be obtained experimentally for solid propellant combustion and this is where mesoscale simulations of combustion come at that point. Direct simulations at particle scale are expected to give the relevant information needed to estimate those three input data as it will be addressed in Section 3.

Before moving to propellant combustion simulations, we present basic validations and outcomes from the combustion noise model described above. Figure 1 shows an example of a synthetic turbulent noise using input parameters Λ_e=0.4 mm, Λ_t=5 ms and u_{rms}=0.4 m/s. The left panel plots the normal velocity fluctuation $u'(x)$ as a function of position x along the propellant surface (here, 5 mm for this test) whereas the right panel shows a probability density function (pdf) computed on 10^6 realizations. The pdf has a Gaussian shape with a quasi-zero average $\langle u' \rangle$= -0.003 m/s and standard deviation $\langle u'^2 \rangle^{0.5}$ = 0.39 m/s close to the prescribed value (0.4 m/s). This Gaussian shape is expected here because the length of the domain (5 mm) is quite large compared to the noise correlation length Λ_e=0.4 mm. Because the noise is space-correlated, the Gaussian behavior is not expected if we focus on distances smaller or on the order of Λ_e.

DOI: 10.13009/EUCASS2017-144

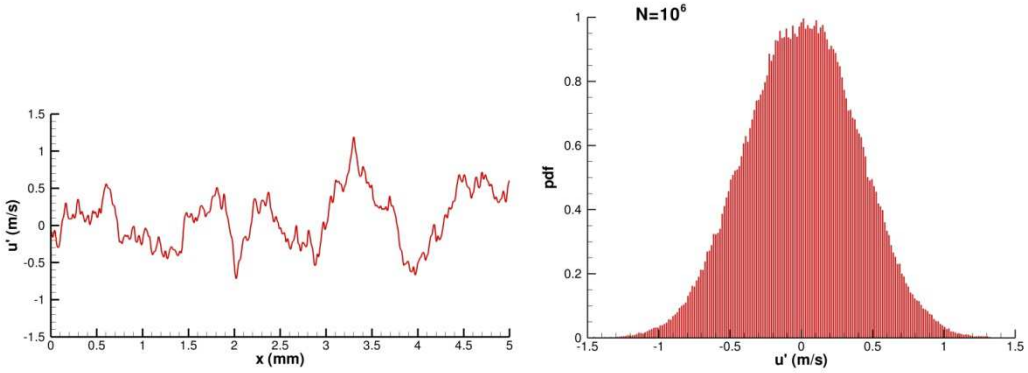

Figure 1: Example of synthetic noise: space variation (left) and probability density (right)

The length scale Λ_e and time scale Λ_t can be estimated from time autocorrelation B(τ) and space autocorrelation B(δ) given by [11]

$$B(\tau) = \frac{\int_S \int_t u'(\mathbf{r},t).u'(\mathbf{r},t-\tau)dtdS}{\int_S \int_t u'(\mathbf{r},t).u'(\mathbf{r},t)dtdS} \qquad B(\delta) = \frac{\int_S \int_t u'(\mathbf{r},t).u'(\mathbf{r}-\boldsymbol{\delta},t)dtdS}{\int_S \int_t u'(\mathbf{r},t).u'(\mathbf{r},t)dtdS} \tag{4}$$

where integrals are performed over time and space. From the velocity signals, both *B(τ)* and *B(δ)* can be computed via Eq. (4) and are presented in Fig. 2. An integral scale can be defined as [11]

$$\Lambda_t = \int_0^\infty B(\tau)d\tau \qquad \Lambda_e = \int_0^\infty B(\delta)d\delta \tag{5}$$

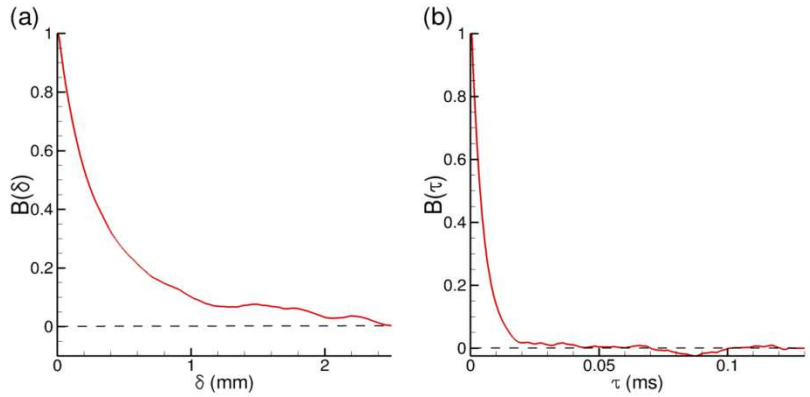

Figure 2: Space autocorrelation B(δ) (a) and time autocorrelation B(τ) (b)

Performing integrals Eq. (5) on results presented in Fig. 2 respectively gives Λ_e =0.42 mm and Λ_t = 4.8 ms, close to what is expected from input data (0.4 mm and 5 ms respectively).

3. Mesoscale simulation of combustion

We now turn to mesoscale simulations of solid propellant combustion in order to evaluate the three unknown input data describing combustion noise, namely velocity amplitude u_{rms} and integral scales Λ_e and Λ_t.We first describe our method briefly since it has already been published elsewhere recently [15,16].

3.1 Model

Our model addresses the combustion of solid propellant at the oxidizer particle scale and is inspired by the seminal works by Jackson et al.[17,18,11]. As mentioned above, more details on the numerical and physical parameters can

DOI: 10.13009/EUCASS2017-144

be found in our recent works [15,16]. The idea is to solve combustion in 3D both in solid and gas phase. The model is developed in an in-house code named COSMETIC.

In the solid propellant, which is supposed inert, only temperature *T* needs to be solved by

$$\rho_c C_c \frac{\partial T}{\partial t} = \nabla . \lambda_c \nabla T \tag{6}$$

Since the propellant is heterogeneous, density ρ_c, specific heat C_c and thermal conductivity λ_c in Eq. (6) vary spatially. In the gas phase, a classical low-Mach development of the Navier–Stokes equations with perfect gas law and unit Lewis number is considered:

$$\begin{aligned}
&\frac{\partial \rho_g}{\partial t} + \nabla . \rho_g \boldsymbol{U} = 0 \\
&\frac{\partial \boldsymbol{U}}{\partial t} + \boldsymbol{U} . \nabla \boldsymbol{U} = -\frac{\nabla p}{\rho_g} + \frac{1}{\rho_g} \nabla . \mu \nabla \boldsymbol{U} \\
&\frac{\partial T}{\partial t} + \boldsymbol{U} . \nabla T = \frac{1}{\rho_g C_g} \nabla . \lambda_g \nabla T + \frac{\dot{\omega}_T}{\rho_g C_g} \\
&\frac{\partial Y_k}{\partial t} + \boldsymbol{U} . \nabla Y_k = \frac{1}{\rho_g} \nabla . \frac{\lambda_g}{C_g} \nabla Y_k + \frac{\dot{\omega}_k}{\rho_g} \\
&\rho_g = \frac{P_0 W}{RT}
\end{aligned} \tag{7}$$

Source terms on species Y_k and temperature *T* are computed based on a BDP kinetic scheme with four species and three reactions [15,16]. Coupling between solid and gas phase is enforced by the following jump conditions at the burning surface:

$$\begin{aligned}
[\rho(\boldsymbol{U} . \boldsymbol{n} + r_b)] &= 0 \\
\left[\frac{\lambda}{C} \nabla Y_k . \boldsymbol{n}\right] &= \dot{m}[Y_k] \\
[\lambda \nabla T . \boldsymbol{n}] &= -\dot{m} Q_s + \varphi
\end{aligned} \tag{8}$$

where brackets denote the jump at the solid/gas interface, **n** is the normal vector at the surface and $\dot{m}$ the propellant mass rate. The heat of decomposition Q_s models the complex reactions taking place at the surface and the additional heat flux φ is here used as an external heat supply for ignition. The position of the solid/gas interface is tracked using the zero-value of a level-set function ψ which satisfies the following Hamilton–Jacobi equation

$$\frac{\partial \psi}{\partial t} + r_b \|\nabla \psi\| = 0 \tag{9}$$

where r_b is the burning rate. Numerical details, physicochemical or kinetic input data can be found in Ref. [15,16].

3.2 Simulations on an AP/HTPB Propellant

This work intends to focus on a typical industrial propellant, which contains 68 % AP (Ammonium Perchlorate), 18 % aluminum, and 14 % HTPB (Hydroxyl-Terminated PolyButadiene). As is, our model currently does not model aluminum explicitly. But since aluminum is not expected to take part to propellant combustion [19], we assume that it can be discarded and we consider an equivalent AP/HTPB propellant by keeping the same AP/HTPB ratio. Therefore, forthcoming simulations are performed on a propellant with 83 % AP/17 % HTPB having bimodal distribution. Coarse AP is supposed to have an average diameter of 200 µm and fine AP is homogenized into the binder. Thus, only coarse AP particles are explicitly modeled as a sphere pack. We have considered monodisperse or log-normal distribution for AP but found negligible effects; we here present results obtained with a log-normal distribution. The sphere packs are obtained with a Monte-Carlo algorithm on a cube of size 2.5 mm, replicated several times in the combustion direction.

Simulations are performed at a pressure p=5 MPa, which is typical of motors. The mesh is uniform in homogeneous directions (constant grid spacing of 15 µm) and refined at the surface with grid spacing down to 1 µm. The total number of grid points is approximately 3 million. Figure 3 illustrates such mesoscale simulations with the combustion surface and a gas temperature slice. The surface is corrugated due the burn rate mismatch between oxidizer and binder. There are large fluctuations in temperature depicting different flame structures (diffusion vs. premixed) and, accordingly, large velocity fluctuations as well. This shows how combustion at microscale is far from homogeneity. The simulation is run during at least 0.3 s so that at least one initial pack of size 2.5 mm has been entirely burnt. Velocities and temperature are stored in each computational cell every 1 ms, which leads to 200 GB of data that will be subsequently studied in a post-processing step (see Section 3.3).

DOI: 10.13009/EUCASS2017-144

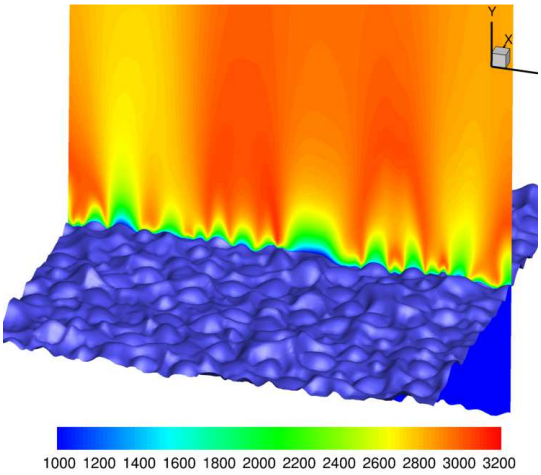

Figure 3: Combustion surface and gas temperature slice (K)

3.3 Data processing

The relevant information here is gas velocity and temperature. Note that although we do not consider temperature fluctuations at that time in our noise model (this will be part of subsequent studies), we however present results on temperature. In CFD simulations of motors, solid propellant combustion is assumed to be a surface process because propellant flame stand-off distances are much smaller than grid size. As a consequence, relevant data for boundary conditions must describe that flow slightly above the surface, away from any reactive zone. More specifically, the gas velocity must be taken out of the combustion zone, to be devoid of any volumetric dilatation effects. When chemical reactions are complete, velocity is relatively constant and driven by the usual non-reactive Navier-Stokes equations. We have found that the reactive zone extends up to 200 µm from propellant surface in present case, so that we will choose a safe distance of y=500 µm above the surface to study fluctuations. Results have been checked to be independent of a particular value of distance y when above approximately 200 µm.

As mentioned previously, fluctuations are mostly normal to the combustion front and tangential fluctuations are found to be approximately five times smaller. Figure 4 presents the pdf of the normal velocity u and gas temperature T. Velocity shows a Gaussian-like distribution with standard deviation u_{rms}=0.31 m/s, which gives a scaled standard deviation $u_{rms}/\langle u\rangle$ = 12 %. The temperature distribution presents an asymmetric Gaussian-shape with $T_{rms}/\langle T\rangle$ = 7.3 %. The distribution is skewed on the right side because of the maximal stoichiometric temperature of about 3100 K for an AP/HTPB mixture.

Figure 5 presents a plot of autocorrelation functions $B(\delta)$ and $B(\tau)$ obtained from the combustion simulations. The space correlation $B(\delta)$ shows an expected decreasing evolution showing that fluctuations of velocity are strongly correlated at small range but uncorrelated at larger distances, typically 500 µm. From Eq. (5), we compute an integral length scale $\Lambda_e \sim 240$ µm. This length scale is typical of oxidizer particles (200 µm), which is not surprising since heterogeneities in combustion are primarily imposed by the larger burning particles. The time correlation $B(\tau)$ shows a rapid decorrelation followed by oscillating negative/positive values. This can be explained by the temporal succession of low burn rate binder/high burn rate AP particles. The time scale is found to be $\Lambda_t \sim 4.8$ ms. Note that oscillations have a period of ~20 ms which is close to a typical particle burnout time ~200 µm / ~10 mm/s = 20 ms.

As a partial conclusion, mesoscale propellant simulations allow to estimate the desired input data of the combustion noise model. For this particular propellant, we have

- $u_{rms}/\langle u\rangle \sim 0.12$
- $\Lambda_e \sim 240$ µm
- $\Lambda_t \sim 4.8$ ms

We have performed additional simulations at lower and higher pressures (respectively, 3 and 7 MPa). It is not described further in this paper but we have actually noticed little differences on $u_{rms}/\langle u\rangle$ or length scale Λ_e. Only the time scale Λ_t seems to vary much with pressure through an expected scaling $\Lambda_t \propto 1/r_b$ with r_b the propellant burning rate.

DOI: 10.13009/EUCASS2017-144

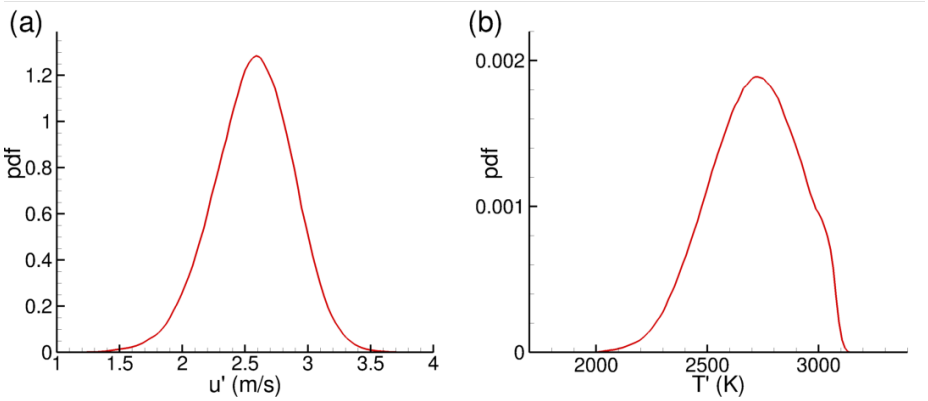

Figure 4: Probability density functions for normal gas velocity (a) and gas temperature (b) for the considered AP/HTPB propellant

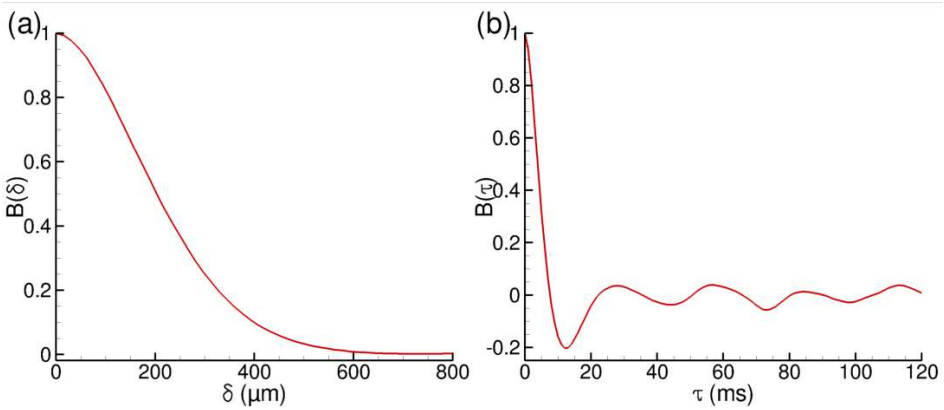

Figure 5: Velocity space autocorrelation *B(δ)* (a) and time autocorrelation *B(τ)* (b) for the considered AP/HTPB propellant

4. Application to subscale motor

In this section, the developed combustion noise model, together with reliable input data from mesoscale simulations, is applied to an actual lab-scale solid rocket motor.

4.1 Description of test case

The present study focuses on a lab-scale solid rocket motor, so-called LP-9, that has been fired in ONERA, Toulouse [20,21]. It is typically 0.7 m long and the burning time is about 2.5 s for an average pressure around 5 MPa. The geometry considered here (labeled #26) is depicted in Fig. 6. It is a simple single-segment cylindrical grain with head-end cavity and submerged nozzle. The motor is unstable at the end of firing on the first longitudinal acoustic mode due to a PVS.

Figure 6: Sketch of LP9#26 labscale motor geometry [20,21]

Computations are performed within a 2D axisymmetric assumption using our in-house CFD code (CPS). Compressible unsteady Navier-Stokes equations are solved with additional perfect gas equation of state. Turbulence

DOI: 10.13009/EUCASS2017-144

is not modeled since the slenderness ratio remains moderate. Boundary conditions for gas injection –modeling the propellant combustion– are taken into account with the described combustion noise model. Simulations are conducted on a fixed geometry (i.e., non-moving) because burnback time scales are very large compared to aerodynamic or acoustic time scales. The geometry considered corresponds to an experimental unstable time (1.9 s after ignition). The computational grid typically involves about 120,000 elements with roughly 1200 points in the axial direction (along motor length) and about 100 points in the radial direction.

4.2 Results

To evaluate the interest of our model, four computations are performed with the following different boundary conditions to model the propellant combustion:

- Constant mass-rate
- Constant mass-rate + small “scotch”
- Constant mass-rate + large “scotch”
- Combustion noise

The first one is the widely-used assumption of a spatially constant propellant mass-rate. The second and third case make use of a “scotch”, basically one or several cells on the propellant boundary condition are imposed at a zero mass-rate. It is only one single cell for the small scotch and five cells for the large scotch, located roughly at mid-grain. This local discontinuity in the mass rate artificially induces some perturbations that are often used to trigger instabilities. The last simulation uses the combustion noise model described previously in this paper.

Results are presented in Tab.1 as instability levels of pressure oscillations (RMS level) at the head-end with experimental data provided as well. The first important information is that a constant mass-rate assumption leads to a stable motor although it is experimentally unstable. As mentioned in the introduction, the modes of PVS instability are temporally damped and they require continuous small perturbations to develop. A single non-injecting cell (small scotch) is enough and the PVS can develop with pressure levels quite close to experiments (88 vs. 74 mbar). The only drawback is that it is unphysical and much dependent on scotch size as seen in Tab. 1 since the five-cell no-injection zone (large scotch) leads to a 60 % increase in pressure level. Clearly, this approach requires unknown arbitrary quantities, which makes it of little interest for predictive simulations. Conversely, the combustion noise model yields reasonable agreement (55 vs. 74 mbar) without any arbitrary parameters. This approach is therefore believed to bring improvements for reliable simulations.

Table 1: Unsteady pressure level depending on boundary conditions (case LP9#26)

	Pressure level (mbar)
Constant	0
Small scotch	88
Large scotch	144
Combustion noise	55
Experiments	74

Figure 7 compares head-end pressure spectra in the case of small scotch and combustion noise. As clear from Fig. 7, the combustion noise model leads to broader and noisier peaks which are qualitatively close to typical experimental spectra. In contrast, very clean and quasi-harmonic peaks are obtained for the scotch case.

DOI: 10.13009/EUCASS2017-144

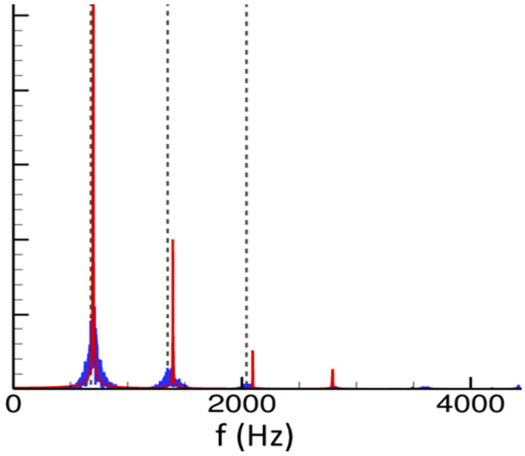

Figure 7: Head-end pressure spectrum: small scotch (red) and combustion noise (blue). The dotted lines are the three first acoustic modes

4.3 Parametric studies

We have conducted additional simulations with the combustion noise model with an eye to evaluating the role of the input parameters: correlation length scale Λ_e, correlation time scale Λ_t and fluctuation amplitude u_{rms}.

Effect of correlation length scale

In addition to the above simulation with Λ_e=240 µm, we have considered a case with a spatially uncorrelated noise Λ_e=0 µm and have noted virtually no effects on the instability. This is relatively expected since the grid spacing on the propellant surface is roughly 0.4 mm. This is slightly larger than the fluctuation scale Λ_e=240 µm, which means that between two neighboring cells fluctuations are only weakly correlated. Going to no correlations at all (Λ_e=0) therefore brings no significant changes.

Effect of correlation time scale

Figure 8 presents the motor instability (head-end pressure level) as a function of the correlation time scale Λ_t (other parameters Λ_e, and u_{rms} are kept at their initial values). Filled symbols are used when the PVS instability is present in the motor (the coherent structures being easily noticed on vorticity fields). Conversely, open symbols note the absence of PVS from numerical vorticity fields. Note the range of time scales, among nine orders of magnitude, from 50 ns (the simulation time step) to 50 s (basically, a time-constant fluctuation). For extreme values of Λ_t, there are no vortical structures apparent in the flow and only a small background noise without clear frequency predominance persists. This means that the instability is not triggered if fluctuations vary too fast or too slowly. For values between 10^{-2} ms and 10^{3} ms, a PVS is noted with clear vortical structures and significant pressure levels. For time scales ranging between 10^{-1} ms and 10^{2} ms, pressure spectra are peakier and much less noisy. Anyway, this clearly shows that PVS needs time-correlated noise to arise but responds to a rather large range of time scales. This means that the exact value of the correlation time scale is moderately important as long as it remains in a reasonable range, say 10^{-1} -10^{2} ms.

Effect of fluctuation amplitude

Finally, we investigate the role of velocity amplitude. From mesoscale simulations, we have taken $u_{rms}/\langle u \rangle$ =12 % and we here consider lower values as plotted in Fig. 9. In all cases (except u_{rms} = 0), there is an instability dominated by a PVS. It is clear from Fig. 9 that the prescribed amplitude has a strong effect on instability levels that increase with amplitude in a logarithmic way. Among the three tested parameters, noise amplitude has the more marked impact and it is therefore important to estimate it correctly for a given propellant and pressure, by using mesoscale simulations for instance. The behavior noted in Fig. 9 is reminiscent of the effect of injected turbulence on pressure levels as already investigated [8]. It is a mere surprise since the noise amplitude is akin to a turbulent kinetic energy.

DOI: 10.13009/EUCASS2017-144

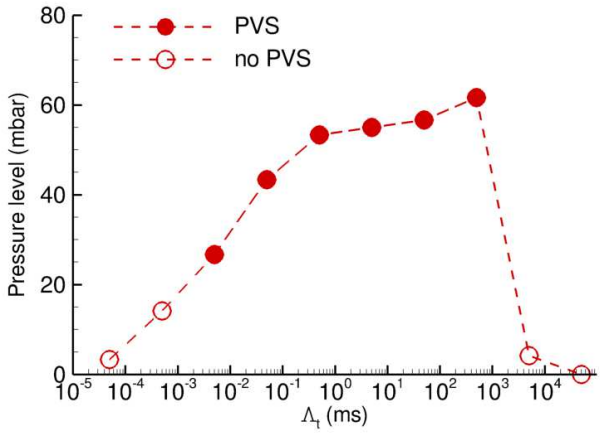

Figure 8 : Head-end pressure level as a function of correlation time scale Λ_t. Filled circles note the presence of a PVS instability in the motor

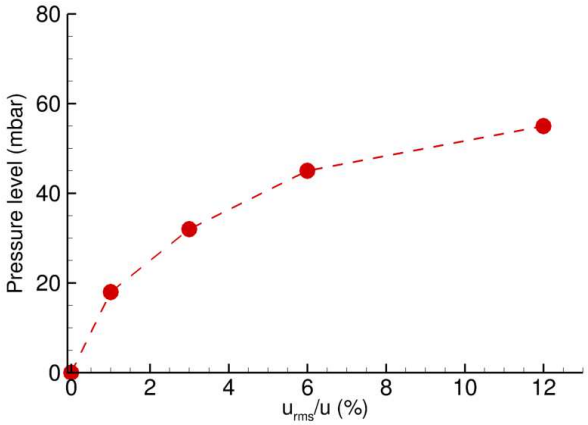

Figure 9 : Head-end pressure level as a function of velocity fluctuation amplitude

5. Conclusions

In this work, we have proposed a “combustion noise” model adequate to represent the velocity fluctuations above the burning surface of a composite AP/HTPB solid propellant. It is based on a spectral synthetic turbulence model as proposed by Davidson et al. [12] and is fully implemented in an in-house CFD solver to be used in large-scale solid rocket simulations at no additional cost. The important input data are the amplitude of the fluctuations as well as their correlation time scales and length scales. Those data are not known experimentally and we propose an estimation based on mesoscale simulations of combustion, an approach already proposed by Jackson et al. [11]. Therefore, mesoscale simulations are performed using an in-house code COSMETIC [15,16]. Since aluminum is not modeled explicitly so far, we have considered an equivalent AP/HTPB propellant representative of typical aluminized industrial propellant. The obtained results gave that velocity fluctuations have an RMS value of ~12 % of the injection velocity, with correlation length ~240 µm (typical of oxidizer particle size) and correlation time ~5 ms (typical of an oxidizer particle burnout time). Simulations on a subscale rocket motor have been performed with this model. It is shown that the model gives physical results, close to experiments, without the need of unphysical arbitrary methods to introduce some randomness.

Future works need to address more experimental cases to assess the relevance of this approach. Considering temperature fluctuations can also be evaluated to obtain a more reliable propellant model to simulate instabilities in solid rocket motors. Finally, the model developed could also be useful to be used with advanced turbulence models or LES to study turbulence in solid rocket motors.

Acknowledgements

This work was supported and partly funded by the French Space Agency CNES (N.Cesco, J.Pichillou).

DOI: 10.13009/EUCASS2017-144

References

[1] Gallier, S., and Godfroy, F. 2009. Aluminum combustion driven instabilities in solid rocket motors. *J.Prop.Power*, 25(2):509–521.

[2] Ballereau, S., Godfroy, F., Gallier, S., Orlandi, O., Thepenier, J., Robert, E., and Cesco, N. 2011. Evaluation method of thrust oscillations in large SRM-application to segmented SRM's. In: *AIAA Paper 2011-6054*.

[3] Najjar, F. M., Ferry, J. P., Haselbacher, A., and Balachandar, S. 2006. Simulations of solid-propellant rockets: effects of aluminum droplet size distribution. *J. Spacecraft Rockets*, 43(6):1258–1270.

[4] Fabignon, Y., Dupays, J., Avalon, G., Vuillot, F., Lupoglazoff, N., Casalis, G., and Prévost, M. 2003. Instabilities and pressure oscillations in solid rocket motors. *Aerosp. Sci. Technol.*, 7(3):191–200.

[5] Gazanion, B., Chedevergne, F., and Casalis, G. 2014. On the laminar-turbulent transition in injection-driven porous chambers. *Exp. Fluids*, 55(1): 1643.

[6] Ciucci, A., Iaccarino, G., Moser, R., Najjar, F., and Durbin, P. 1998. Simulation of rocket motor internal flows with turbulent mass injection. In: *Proc. Summer Prog. Center for Turbulence Research*, Stanford University, 245–266.

[7] Beddini, R. A. 1986. Injection-induced flows in porous-walled ducts. *AIAA J.* 24(11):1766–1773.

[8] Gallier, S., Godfroy, F., and Plourde, F. 2004. Computational study of turbulence in a subscale solid rocket motor. In: *AIAA Paper 2004-4052*.

[9] Chedevergne, F., Casalis, G., and Majdalani, J. 2012. Direct numerical simulation and biglobal stability investigations of the gaseous motion in solid rocket motors. *J. Fluid Mech.*, 706: 190–218.

[10] Casalis, G., Avalon, G., and Pineau, J. P. 1998. Spatial instability of planar channel flow with fluid injection through porous walls. *Phys. Fluids*, 10: 2558–2568.

[11] Massa, L., Jackson, T. L., Buckmaster, J., and Najjar, F. 2007. Fluctuations above a burning heterogeneous propellant. *J. Fluid Mech.*, 581: 1–32.

[12] Davidson L. 2008 Hybrid LES-RANS: Inlet Boundary Conditions for Flows with Recirculation. In: Peng SH., Haase W. (eds) Advances in Hybrid RANS-LES Modelling. Notes on Numerical Fluid Mechanics and Multidisciplinary Design, Vol 97. Springer, Berlin, Heidelberg.

[13] Billson, M., Eriksson, L. E., Davidson, L. 2003. Jet noise prediction using stochastic turbulence modeling. In: 9th AIAA/CEAS Aeroacoustics Conference and Exhibit, Paper 2003-3282.

[14] Durand, P. *et al.* 2000. CPS: A Three-dimensional CFD Code Dedicated to Space Propulsive Flows", In: *36th AIAA Joint Propulsion Conference and Exhibit*, 2000-3864.

[15] Plaud, M., Gallier, S., and Morel, M. 2015. Simulations of heterogeneous propellant combustion: Effect of particle orientation and shape. *Proc. Comb. Inst.*, 35(2): 2447–2454.

[16] Gallier, S., Ferrand, A., and Plaud, M. 2016. Three-dimensional simulations of ignition of composite solid propellants. *Comb. Flame*, 173: 2–15.

[17] Jackson, T. L., and Buckmaster, J. 2002. Heterogeneous propellant combustion. *AIAA J.* 40(6): 1122–1130.

[18] Massa, L., Jackson, T. L., and Short, M. 2003. Numerical solution of three-dimensional heterogeneous solid propellants. *Combust. Theor. Model.*, 7(3): 579–602.

[19] Lengelle, G., Duterque, J., and Trubert, J. F. 2000. Physico-Chemical Mechanisms of Solid Propellant Combustion, In: *Solid Propellant Chemistry, Combustion, and Motor Interior Ballistics*, edited by Yang, V., Brill, TB, and Ren, Wu-Zhen. *AIAA Progress in Astronautics and Aeronautics*, Vol. 185.

[20] Gallier, S., Prevost, M., Hijlkema, J., and Roumy, M. 2009. Effects of cavity on thrust oscillations in subscale solid rocket motors. In: *AIAA Paper 2009-5253.*

[21] Prevost, M., Godon, J. C., and Innegraeve, O. 2005. Thrust oscillations in reduced scale solid rocket motors Part I: experimental investigations. In: *AIAA Paper 2005-4003*